Chapter 2

An Autonomous Receiver/Digital Signal Processor for Wave Experiments: The Dartmouth Rx-DSP

2.1 Introduction

Instabilities in space plasmas produce waves in a wide range of frequencies and bandwidths, with a large variety of time signatures, detectable both in situ and remotely. Detector technologies include inductive loops for magnetic fields, double probes for electric fields, and Langmuir probes for plasma density. For receivers, the ideal wave analysis instrument would involve a direct high-frequency analog-to-digital (ADC) sampling of the output of a given detector or antenna, with the highest possible sampling rate and bit depth. While technology has advanced in recent years to allow continuous sampling at 20 MHz or beyond, it is often not feasible to use such techniques directly, due to limited data transmission and storage capabilities.

Furthermore, it is often desirable to record wave data from multiple detectors simultaneously, e.g. from spatially separated or orthogonal antennae. Such measurements can allow detection of wave polarization and propagation directions. Simultaneous sampling requires a high degree of ADC sample synchronization across multiple receivers, and results in even greater demands on data storage and transmission systems, rendering direct simultaneous sampling even less attractive.

Data storage and transmission limitations are at their most severe on spacecraft, and therefore many innovative solutions have come out of that community. For example, the Cluster satellites, launched in 2000, included the Wide-Band plasma investigation (WBD). This instrument was capable of downconverting in selected frequency bands, removing the need for storage of samples at twice the Nyquist rate (*Gurnett et al.* 1997). Another example is the

Waves instrument onboard the Van Allen Probes (formerly RBSP), launched August 2012, which is similar to the WBD, but also allows for dynamic Fast Fourier Transforms (FFTs) and data compression (*Kletzing et al.* 2013). The receiving system most similar to the subject of this chapter is the Radio Receiver Instrument (RRI) on board the e-POP payload of the Canadian CASSIOPE satellite. The RRI directly samples four probes at 40 MHz and then performs on-board signal processing (*James et al.* 2015).

The Dartmouth Receiver/Digital Signal Processor (Rx-DSP) represents another recent development effort to address these issues. As a digital downsampling receiver, it can transmit wave data within a specific band or set of bands within the 0 to 33 MHz range. The data can be sampled either continuously or in bursts, allowing for fine-grained customization of the transmission data rate. In addition, the Rx-DSP boards are designed for cross-receiver sample synchronization to within 2 nanoseconds. The Rx-DSP is set apart by its autonomous capabilities with remote reprogrammability, high maximum sample rate, and myriad options for data transmission. The generalized nature of the instrument front-end allows for use with a wide range of detector hardware. It also allows for a variety of both spacecraft-borne and ground-based applications, as discussed below.

Section 2.2, describes the current iteration of the Dartmouth Rx-DSP hardware, and Section 2.3 explains the naming convention for individual deployments. Section 2.4 provides an overview of the firmware used on the onboard programmable DSP. Finally, Section 2.5 presents three examples of applications of this system to space physics, with case studies of one rocket mission and two ground-based detectors.

2.2 Hardware

The Rx-DSP is a low-cost analog-to-digital receiver and signal processor board, designed for use in both ground and space scenarios, and specifically engineered for cross-board sample-synchronized acquisition. The use of purpose-specific receiver components allows for a significant shortening of system development cycles as compared to an FPGA-based solution, by removing programming, testing, and debugging complexities; however, the specific components chosen for the Rx-DSP platform maintain appreciable flexibility in the field. The detailed architecture of the boards has sounding rocket flight history from instruments produced at the University of Iowa. The current generation of boards have been tested for reliable operation at temperatures from 0 to 50 C—more extreme ground environments require external regulation, such as placement in insulated or heated boxes, whereas sounding rockets are warmed on the launch pad, and flights are not long enough for cooling to be a concern. While the Rx-DSP design could be extended for high-radiation space environments, this has not been a goal of current development efforts. Data acquisition systems incorporating the Rx-DSP are easily crafted for autonomous operation with no external command and control, transmitting results via a number of protocols. Figure 2.1 shows a picture of the topmost Rx-DSP board in a stack of two—a configuration used in several applications. The data flows through the board as in Figure 2.2, going through asynchronous Receive, Processing, and Transmit stages.

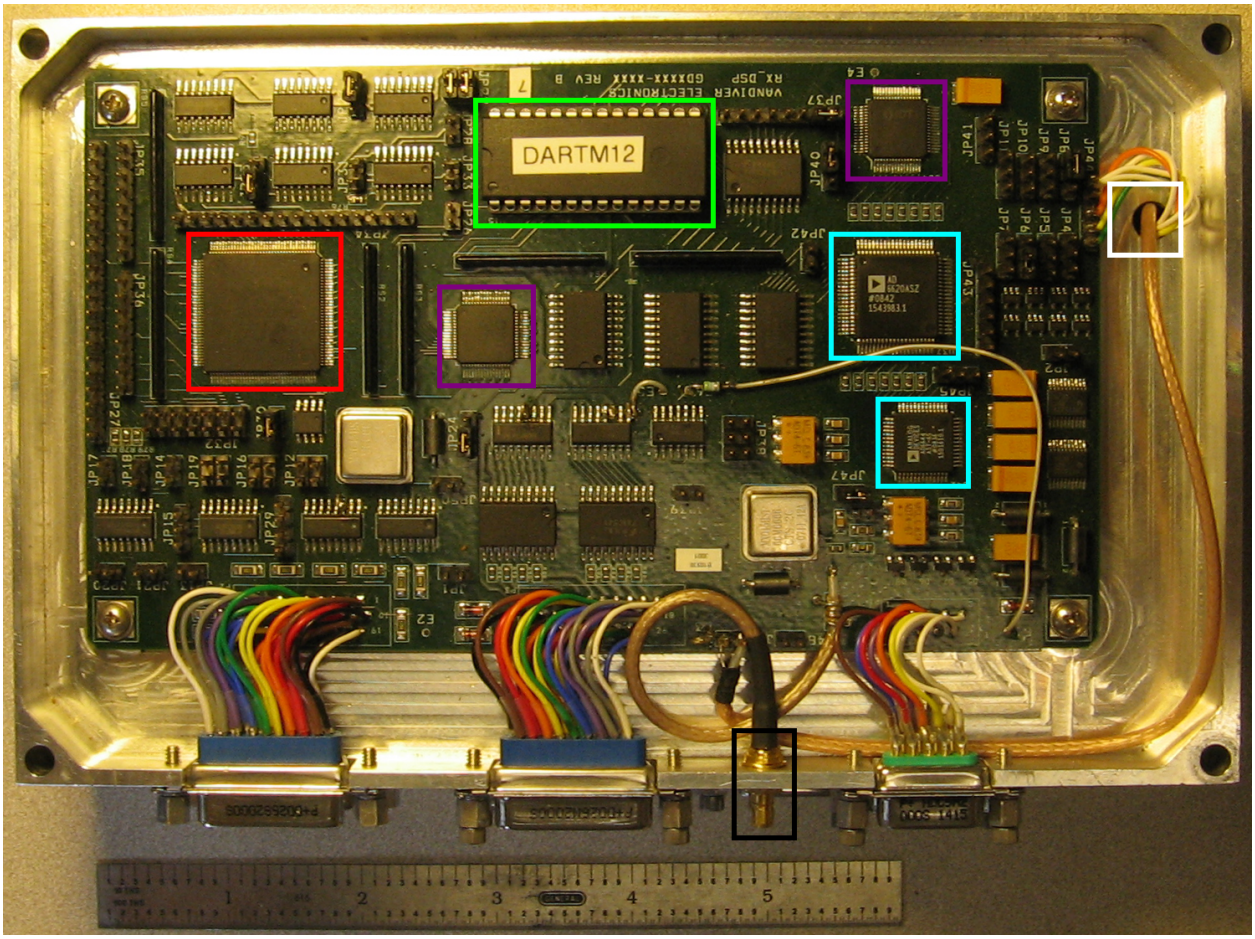

Figure 2.1: A photograph of the top board of an Rx-DSP stack ready for a rocket flight, with 6 inch ruler for scale. Highlighted are the SMB signal input (black), cross-board synchronization lines (white), AD6644 & AD6620 signal processors (cyan), IDT72285 FIFOs (purple) TMS320C542 programmable processor (red), and the program-code EEPROM (green).

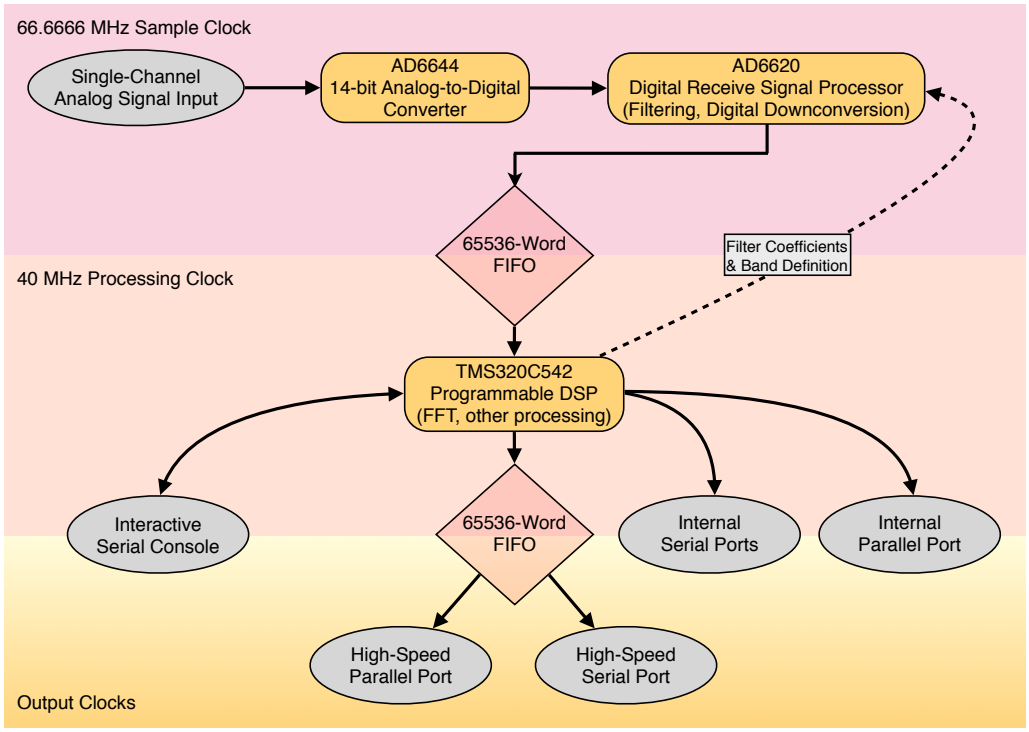

Figure 2.2: A diagram depicting the major parts of the Rx-DSP hardware, and the data flow between them, with the dashed line indicating command/control and solid lines indicating data or both. The colored background boxes indicate which systems are controlled by which clocks.

The Receive stage takes a balanced analog signal with a maximum 1 volt peak-to-peak amplitude, fed to the input of an Analog Devices AD6644 ADC, which samples at 66.6666 MHz with 14-bit resolution, yielding a 33.3333 MHz Nyquist frequency, 74 dB signal-to-noise ratio (SNR), and 100 dB spurious-free dynamic range. There is no built-in filtering, and an input bandwidth of 250 MHz, allowing for undersampling downconversion; thus, each application requires customized front-end pre-amplifiers and filters for band-limiting and antialiasing. The outputs of the 6644 are linked directly to an Analog Devices AD6620 programmable digital Receive Signal Processor (RSP). This processor performs quadrature frequency translation, and then decimates and filters the incoming signal through three stages, yielding a band with width, center, and filter characteristics defined by a table of values and filter coefficients. The RSP can further improve the SNR, and the total system performance and frequency response will be unique to each application, determined by the preamplifiers, filters, and cabling used. The quadrature data is output from the RSP as 16-bit words, with In-phase and Quadrature (I and Q) words being interleaved, and each word is accompanied by a bit which indicates whether a given sample is an I or Q word. This relatively low-frequency, 17-bit data is then stored to an 18-bit Integrated Device Technology IDT72285 First-In First-Out (FIFO) buffer.

The receive FIFO output is accessible to a Texas Instruments (TI) TMS320C542 Digital Signal Processor. This processor has a number of useful built-in peripherals, runs on an external clock (generally set for 40 MHz operation), has 10 kilowords of built-in RAM, and can access up to 16 KB of program code and tables from an external PROM. In many deployments, this DSP acts only as a data router and packager, adding headers and/or synchronization information before passing the data onwards. However, by loading custom software to this processor, a variety of real-time, streaming data processing effects are achievable, such as FFTs and various types of compression, though no such deployments will be shown in the case-studies herein.

After all desired data processing steps are complete, the data in memory can follow a number of output paths. First, the data can be sent at high speed to a second IDT72285 FIFO. The outputs of this FIFO are accessible to high-speed serial and parallel LVDS outputs, at any speed up to the full quadrature data rate. A second option can exploit one of two serial ports available on the TMS320C542: a buffered serial port that allows efficient data transfer at standard RS-232 speeds, and a time-division multiplexed port that allows multiple boards to share one serial link. A third option makes use of a parallel Host Port Interface that allows the DSP to connect to an external device at high speeds (up to 8 MBps). Finally, a fourth possibility is to wire and program the Rx-DSP to allow dropping to a single-line interactive serial console, through which a user can trigger single acquisitions, read data, configure settings, or remotely re-burn the firmware EEPROM.

In many use cases, the DSP is able to spend idle time in a low-power mode, significantly reducing the average power draw of the Rx-DSP board—without detailed optimization, the power draw per Rx-DSP is approximately 1.5 W. The flexibility in configuration, coding, and data output allow for a wide range of receiver setups. In addition, the AD6620 is designed to allow for sample synchronization across chips, and the Rx-DSP boards are designed to allow the sample clocks and RSPs to be synchronized as well, using short (< 10 cm) jumper

wires which pass the clock and AD6620 synchronization lines between boards. This allows for the development of multi-board setups for wave-polarization measurements and direction finding.

2.3 Nomenclature

Each individual deployment of Rx-DSP hardware requires custom hardware for input refinement, power, command input, and data output. For ease of referral, each Rx-DSP system may be referred to as an **A**utonomous **R**x-DSP **C**luster (ARC), with a prefix signifying current data collection intent. The current set of prefixes are arrayed below:

1. P - Polarization
2. F - Fine Structure
3. M - Multi-Band
4. I - Imaging/Direction-Finding
5. S - Spectrum Analyzing

The other element which is generally different in each ARC is the firmware loaded by the TMS320C542 processor.

2.4 Firmware Overview

The limited RAM on the TMS320C542 processor is shared between loaded programs and data, requiring careful management of program size and data storage. The programs used are all hand-coded in TI DSP Assembly, except for the FFT module, which is based on code from the TI DSP C Library. The default mode upon power-up has the DSP load its program code from the onboard PROM and then commence execution.

The program code developed at Dartmouth for rocket and ground-based application is modular, but all implementations follow a general structure outlined in Figure 2.3. After initializing the C542 and AD6620 hardware, the AD6620 acquisition is started, and data is loaded into RAM by the C542. For continuous high-speed data acquisition, the AD6620 may be left 'on'; however, when only discrete data blocks are required, power usage can be cut significantly by halting acquisition between blocks.

Once the data is in RAM, any number of processing steps can apply, limited only by available RAM and processing time. In the simplest case the data is untouched. In the most complex case currently coded, 1024-word FFTs are performed on incoming data. For most cases, the data is next encapsulated in a synchronization framework, which includes sync words, sampling-specification headers, and frame counters. The processed data is next prepared for output.

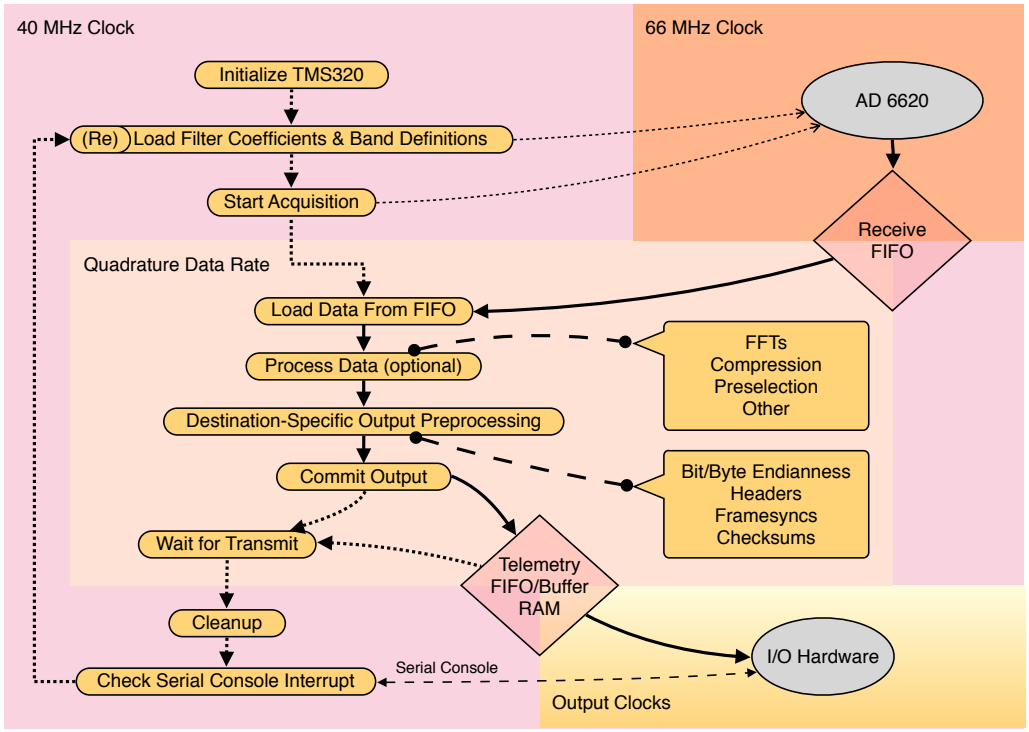

Figure 2.3: A diagram depicting a generalized program flow for the Rx-DSP assembly code. Dashed lines indicate command/control flow, while solid lines include data as well. Color backgrounds show which parts of the code run at the given clock rates, with FIFOs and wait cycles allowing for asynchronous operation. The two callout boxes show modularized routines in the codebase, some, all, or none of which may be used by a given ARC.

Data handling for output varies widely, depending on final destination, DSP setup, and output hardware. To output to the high-speed serial or parallel systems, data is merely copied into the output FIFO and then read out via rocket telemetry or PC USB hardware. For output involving the C542 chip's built-in peripherals, various preprocessing steps may be required, including downsampling, data subset selection, endianness conversion, and the addition of extra sync data and headers. The most efficient C542 peripheral for data output is the Buffered Serial Port, which merely requires that its rotating buffer is periodically filled. All other peripherals require that each byte be individually preloaded. In either case, data loading can either be handled by fixed software loops, or can be interrupt driven.

A special case for input and output on the DSP is the software serial console interface. This link allows a PC with a standard RS-232 serial port to connect to the C542, which can be switched into the serial console mode via an external toggle. The console allows for single acquisitions, direct editing of program code in RAM, modifications to the AD6620 setup, and for the uploading and burning of new PROM files for permanent changes.

2.5 Case Studies

2.5.1 CHARM-II – Rocket-Borne Application

Auroral roar is a natural ionospheric radio emission characterized by a relatively narrow-banded structure centered at frequencies near multiples of the electron cyclotron frequency. It is most frequently observed by ground-based radio receivers, but has also been seen by satellites (*James et al.* 1974; *Benson and Wong* 1987; *Bale* 1999). The intense electrostatic upper-hybrid waves which are the source of auroral roar have been detected by a sounding rocket, but hitherto not the auroral roar itself (*Samara et al.* 2004). Detailed ground-based studies have shown that many instances of roar are not singular emissions, but rather contain intricate fine structures visible on high-resolution frequency-time plots (*LaBelle et al.* 1995; *Shepherd et al.* 1998b). Further studies have determined that the lowest harmonic of roar seen on the ground ($2f_ce$) is left-hand elliptically polarized with respect to the local magnetic field (*Shepherd et al.* 1997), while there have been observations of higher harmonics being either left or right-hand polarized (*Sato et al.* 2012). It is theorized that roar originates as upper-hybrid plasma waves above the ionospheric 'F peak', converting through linear or nonlinear processes into propagating electromagnetic waves (*Shepherd et al.* 1998a; *Yoon et al.* 2000; *Ye et al.* 2007), and the HIBAR and Porcupine sounding rockets may have encountered regions of such plasma waves (*Carlson et al.* 1987).

The Correlation of High-Frequency and Auroral Roar Measurements (CHARM-II) auroral sounding rocket carried the second successful deployment of the Rx-DSP hardware. On the CHARM-I mission the Rx-DSPs returned approximately 1-2 minutes of data from exposed, partially deployed electric-field probes, before these probes sheared off due to catastrophic payload failure. The CHARM-II mission was launched from the Poker Flat Research Range near Fairbanks, AK, at 9:49 UT/22:46 MLT on 16 February 2010, reaching an apogee of 802 km. The payload carried a two-board FP-ARC, each receiver digitizing the differential

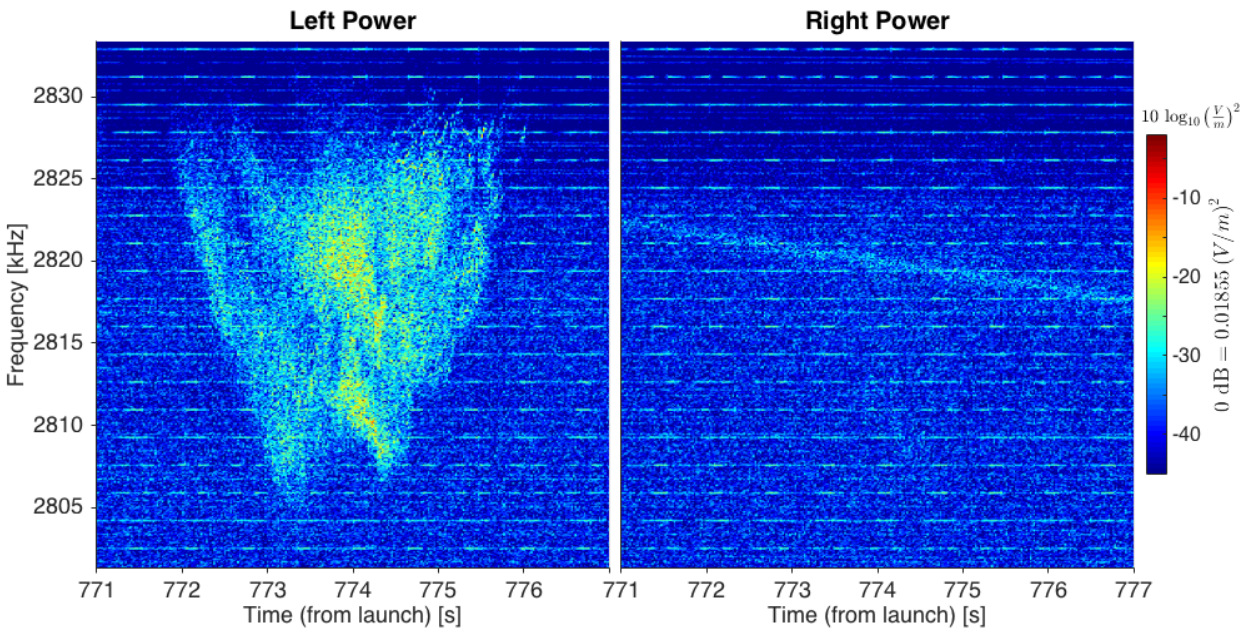

Figure 2.4: Power spectra of Rx-DSP data from CHARM II, recombined to yield left- and right-circularly polarized powers. The line of power with decreasing frequency seen in the righthand plot is an interference line of unknown origin which exists through much of the flight, and has been seen on other flights.

voltage between two 2.5 cm spherical aluminum probes, with the two probe sets positioned perpendicular to each other in the plane orthogonal to the rocket's spin axis, which was oriented parallel to the geomagnetic field. The Rx-DSPs were in a simple downsampling mode, adding short headers and outputting through the high-speed telemetry FIFO and LVDS serial link. The data rate was set to maximally utilize two S-band telemetry links, transmitting downsampled data in a 333 kHz band centered at 2.67 MHz. As the payload nominally had its spin axis aligned with the Earth's magnetic field, $\boldsymbol{B}$, the Rx-DSPs in this configuration effectively yielded a picture of the projection of electric-field wave activity onto the plane perpendicular to $\boldsymbol{B}$ within the designated band.

The CHARM-II FP-ARC yielded the first in-situ observation of auroral roar with both high time resolution and polarization data. Figure 2.4 shows spectrograms over a 298 to 330 kHz band from 771 to 777 seconds after launch, corresponding to 548 to 536 km altitude on the downleg of the flight. The color scale represents the power of righthand circularly polarized signals (a) and lefthand circularly polarized signals (b), with polarizations being with respect to $\boldsymbol{B}$.

Figure 2.4 was generated using a technique described by *LaBelle and Treumann* (1992), adapted from *Kodera et al.* (1977). Given time series data corresponding to two perpendicular, transverse components of a field, as from the measured X and Y components from the Rx-DSPs, a spectral power can be estimated for lefthand and righthand circular wave polarization by recombining the complex Fast Fourier Transforms (FFT) of the time series,

according to

$$FFT_L = FFT_X + \imath \times FFT_Y,$$
$$\text{and} \quad FFT_R = FFT_X - \imath \times FFT_Y.$$

For the CHARM II data, the two perpendicular quadrature signals are detected in situ, and transmitted to ground via payload telemetry systems. In post-flight processing, the data is FFTed, and then recombined to yield the estimated left and righthand powers shown in Figure 2.4.

Figure 2.4 clearly establishes that the observed waves are lefthand polarized. Not only does this confirm the ground-level observations of *Shepherd et al.* (1997), it expands upon it, as the high time and frequency resolution makes it clear that the individual fine structures are all lefthand polarized. *Sato et al.* (2015) have performed a similar analysis for ground-level $4f_{ce}$ roar emissions. The lefthand polarization of these waves is consistent with various generation theories, especially those put forth by *Yoon et al.* (2000).

2.5.2 South Pole Station – Ground-Based Application

South Pole Station (SPS) lies on the Antarctic Plateau thousands of kilometers from commercial and other broadcast activities associated with population centers. As a result, the station is very favorable for studies of radio emissions of natural origin, and hosts a variety of radio receivers at ELF to HF frequencies, complemented by other geophysical diagnostics such as all-sky cameras, photometers, and flux-gate magnetometers. Significant observations at VLF (*Martin* 1960; *Chevalier et al.* 2007), LF-MF (*LaBelle et al.* 2005; *Ye et al.* 2006; *Yan et al.* 2013; *Broughton et al.* 2014), and HF (*Rodger and Rosenberg* 1999; *Patterson et al.* 2001) have been made at the station.

Hence, it was a natural decision to deploy the Rx-DSP to the South Pole. In January 2012 Dartmouth installed a PF-ARC at SPS, consisting of two Rx-DSP boards wired to perform synchronized sampling. Two 40 m^2 loop antennas perpendicular to each other, supported by a 10 m mast, were constructed about 1 km from the station. Figure 2.5a shows these antennas. The planes of the loops are perpendicular to the ground and to each other, providing highest sensitivity to waves coming from overhead, and allowing right- and left-hand polarization to easily be distinguished from the phase relation between the signals. The ARC, a duplicate of that shown in Figure 2.5b was programmed for continuous sampling of a 330-kHz band centered on 515 kHz. Data were offloaded to a PC through the Rx-DSP parallel LVDS link via a pair of QuickUSB high-speed USB data acquisition modules, and stored on an array of 2 TB hard drives. Spectral and cross-spectral analysis of the signals on the Linux computer determined power and polarization of all signals exceeding the noise level. All computer hardware as well as the ARC were housed in an insulated box as in Figure 2.5c, designed to retain waste heat, keeping them within their operating temperature range after installation in the unheated V8 science vault at SPS.

Figure 2.6 shows spectrograms recorded by this ARC on two days in 2013: July 8 and August 2. In both cases, five minutes of data from one of the two signals are shown, and the data come from within 1.5 hours of magnetic midnight, which occurs at 03:35 UT at

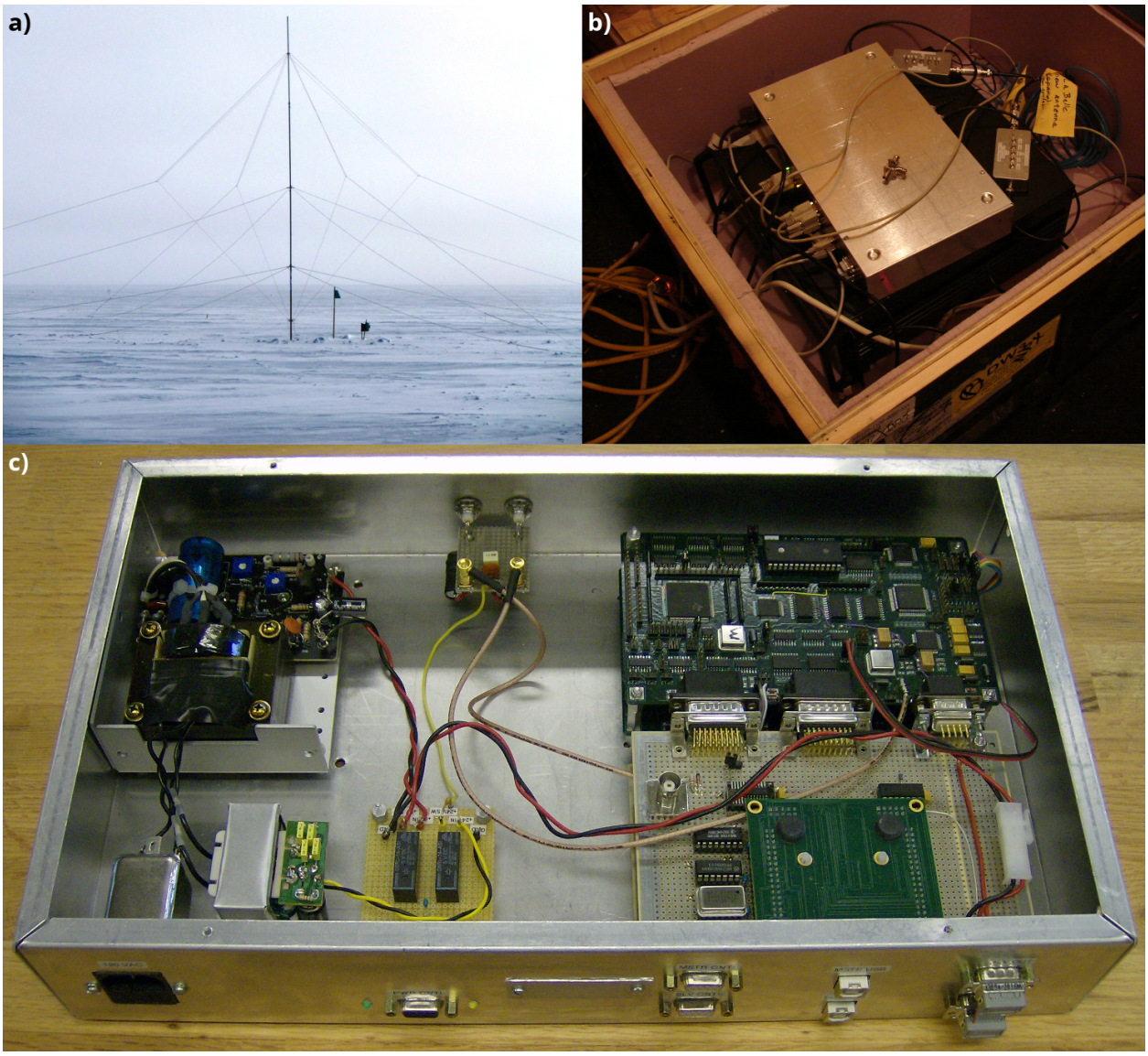

Figure 2.5: Photos of the various components of the South Pole Station PF-ARC. Top left shows the crossed-loop antenna with a 30 ft mast, and the pre-amplifier at the base. Top right shows the receiver box, data-acquisition PC, and various other equipment within an insulated box (covered when in operation). Bottom shows a lab-bench photo of a PF-ARC, with two vertically stacked, sample-synchronized Rx-DSP boards and adjoined QuickUSB breakout boards on the right side.

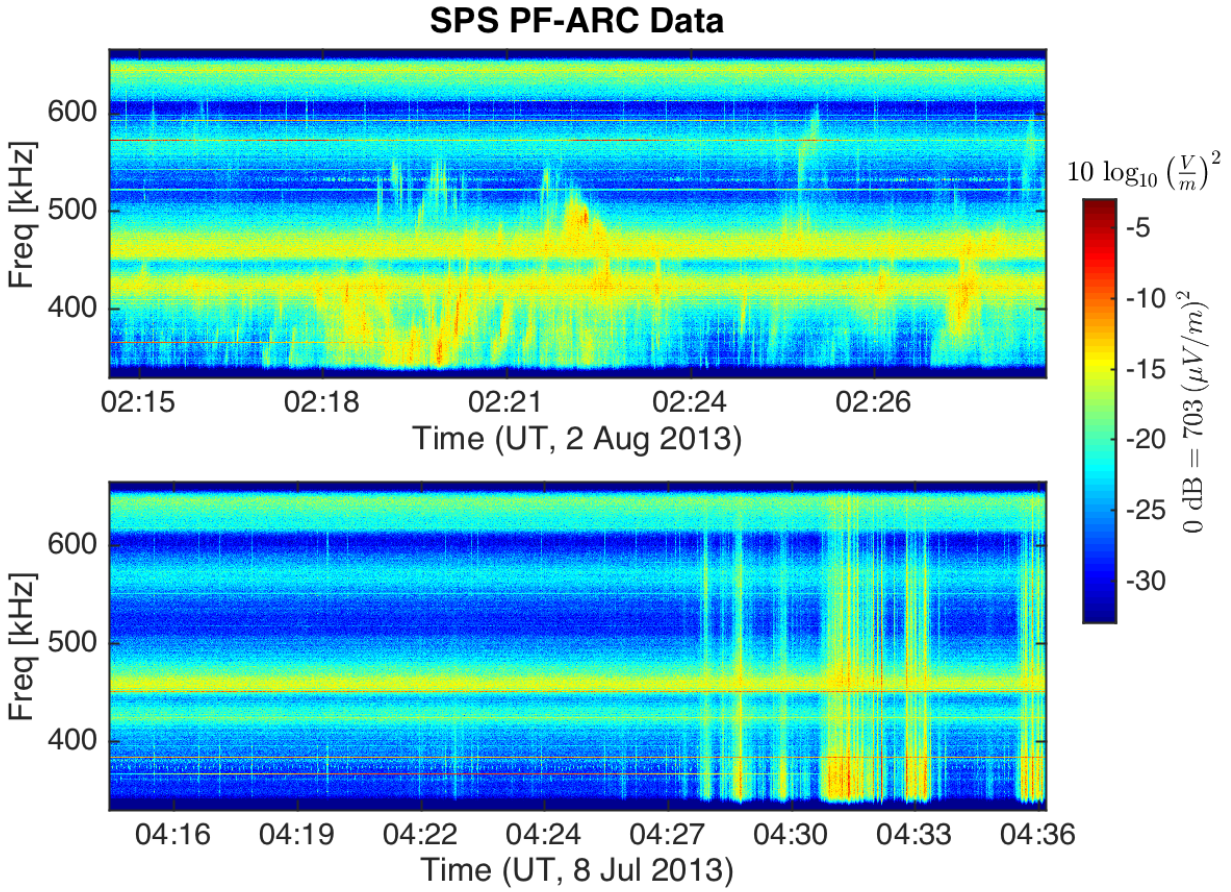

Figure 2.6: Results from the PF-ARC at South Pole Station. The upper spectrogram shows fine structures in signals which appear similar to Auroral Kilometric Radiation, while the lower plot shows an example of auroral hiss, for comparison.

South Pole. In both spectrograms, sharp decreases in the signal power spectral density near the band edges show the effectiveness of the digital filtering in the RX-DSP which defines the bandwidth. Despite the remoteness of South Pole Station, activities at the station lead to strong interference lines, most prominently at 450-460 kHz and 640-650 kHz in each spectrogram and somewhat more weakly at 570-580 kHz and 420-430 kHz.

However, between these interference lines, both spectrograms show evidence of natural radio emissions of auroral origin. The bottom panel, from July 8, 2013, shows a phenomenon called auroral hiss (*Makita* 1979; *Sazhin et al.* 1993; *LaBelle and Treumann* 2002). The high resolution Rx-DSP data show that at LF the hiss consists of impulsive emissions appearing as vertical lines on the spectrogram.

The top panel, from August 2, 2013, shows a phenomenon called 'AKR-like emissions' (*LaBelle and Anderson* 2011; *LaBelle et al.* 2015). This phenomenon is characterized by complicated fine frequency structure consisting of rising and falling tones with typical slopes of hundreds of Hz per second. These features qualitatively resemble those observed in outgoing

X-mode auroral kilometric radiation (AKR) detected with satellite-borne receivers at great distances from Earth (*Gurnett and Anderson* 1981). As pointed out by *LaBelle et al.* (2015), the strong resemblance between this phenomenon and AKR, combined with the stark differences between it and the auroral hiss shown in the top panel of Figure 2.6, forms a powerful argument for a connection between the ground-level AKR-like emissions and the outgoing AKR observed in space.

Due to the success of these observations, further experiments are planned with the Rx-DSP at South Pole. For example, in Summer-Fall 2014 and Summer 2015, the South Pole ARC was operated during anticipated conjunctions between it and Cluster satellites, with the Cluster wave instrument tuned to the same frequency band, in hopes of detecting identical fine structure in ground and in space. Furthermore, as described above, an S-ARC which can perform live spectrum analysis is being installed in Automatic Geophysical Observatories. These autonomous digital receivers in the low-noise Antarctic environment show promise to make important advances in understanding radio waves of auroral origin.

2.5.3 Sondrestrom Research Facility – Ground-Based Application

The Sondrestrom Research Facility lies on the southwest coast of Greenland near Kangerlussuaq, at 66.99° N 309.06° E and is home to numerous instruments for researching Earth's upper atmosphere. These include an incoherent scatter radar, allsky imagers, riometers, magnetometers, and various radio receivers. The MI-ARC at this site consists of a trio of sample-synchronized Rx-DSPs. Input to these comes from five loop antennae: one reference, two situated 50 m from this along lines perpendicular to each other, and two more at 400 m from reference along the same lines. The antennas are arrayed in a small valley approximately 1 km from the station. The three-board MI-ARC is installed in an unheated vault next to the reference antenna, with the receiver itself in a heated, insulated box. The only connection from the vault to the station is a single coaxial cable, which carries both the serial digital output of the ARC, and DC voltage that powers the ARC. The entire array is calibrated at installation and after any major system changes or repairs, through observation of analog reference signals with known strengths and physical source positions.

The ARC triggers relays to switch between the 50 m and 400 m antenna pairs when digitizing signals above and below 1 MHz, respectively. The DSPs are set for discrete sampling of 750 kHz bands, with the receivers rotating through a set of four center frequencies (475, 1225, 1975, and 2725 kHz) approximately once per second. The data are offloaded through the buffered serial port, interleaved via a hardware serial multiplexer, and then transmitted via RS-232 serial link to a remote PC.

To compute the direction of arrival for incoming signals, the three resultant data streams are combined pairwise through cross-spectrum analysis, and averaged over eight 128 or 512-bin FFT ensembles. Then, given calibration data and knowledge of the antenna layout and cable lengths, the phase delays of the resulting spectra can be used to calculate the direction of arrival of high-coherence signals.

Figure 2.7 shows an example of such an analysis for 14 Sep 2013, using signals from 1-1.5

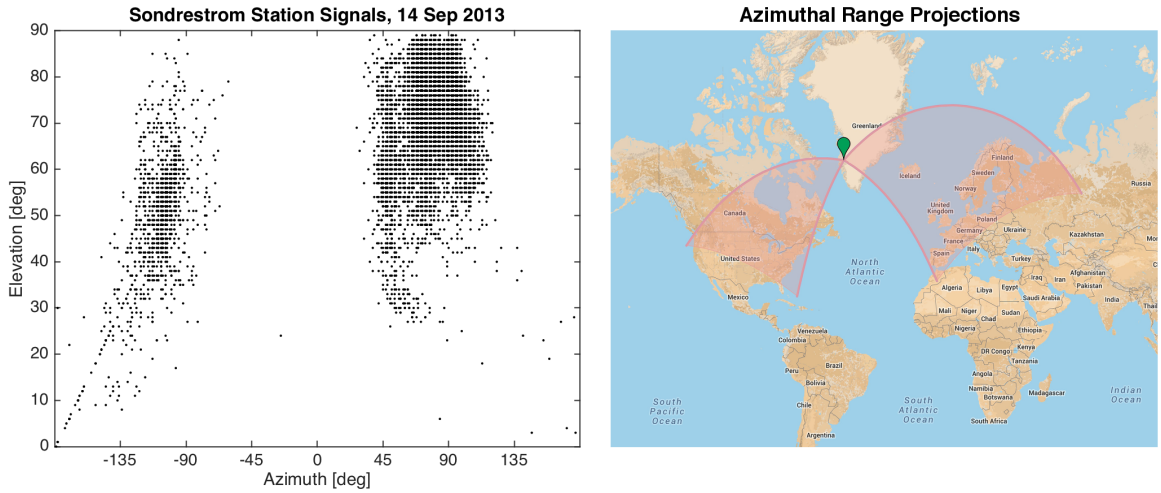

Figure 2.7: Proof of functionality for the MI-ARC at Sondrestrom Station. To the left, an elevation vs. azimuth scatter plot (elevation from the horizon, azimuth in degrees from true north) of high-coherence points for 14 Sep 2013, showing two clear clusters of points. To the right, we project the azimuthal ranges of the two clusters onto a map, implying that the clusters correspond to signals transmitted from Europe and North America [Map data ©2015 Google, INEGI].

MHz with coherence greater than 0.95. The scatter plot above shows elevation vs. azimuth for over 10,000 signals, where elevation is degrees off the horizon and azimuth is degrees from true north. Note that various instrumental uncertainties yield about a 5% uncertainty for each point. The accompanying map shows the approximate azimuthal extent of the two clusters of points. It is clear that the signals detected originate from the directions of North America and Europe. One curiosity is the extension of North American signals to lower elevations, which implies sensitivity to more distant signals. This may be due to atmospheric inhomogeneities or field-of-view anisotropy.

These results establish that the Sondrestrom receiver array/MI-ARC produces accurate direction finding with high time and frequency resolution. The system is resource-efficient, operating autonomously and remotely via a single 1 km coaxial data/power cable. Further data collection for science purposes is ongoing.

2.6 Summary

The Rx-DSP is a flexible platform for high-frequency geophysical data acquisition. ARCs are able to be crafted for autonomous operation in extremely remote regions, for low power draw, and for a wide variety of data transmission rates and media. In particular, the potential for on-board data analysis, reduction, selection, and compression allows for optimal use of low-bandwidth telemetry systems. Additional deployments are already underway, and future revisions of this platform should allow for even more diverse uses.

Thanks to J. C. Vandiver for hardware and firmware development and maintenance, and to Spencer Hatch for presenting this instrument at the 2015 Conference on Measurement Techniques in Solar and Space Physics.

Bibliography

Bale, S. D., Observation of topside ionospheric mf/hf radio emission from space, *Geophys. Res. Lett.*, *26*(6), 667–670, 1999.

Benson, R. F., and H. K. Wong, Low-altitude isis 1 observations of auroral radio emissions and their significance to the cyclotron maser instability, *J. Geophys. Res.*, *92*(A2), 1218–1230, 1987.

Broughton, M. C., J. LaBelle, and P. H. Yoon, A new natural radio emission observed at south pole station, *J. Geophys. Res.*, *119*(1), 566–574, doi:10.1002/2013JA019467, 2014.

Carlson, C. W., R. E. Ergun, A. J. Mallinckrodt, and G. Haerendel, Observations of intense electron bernstein wave emissions in an auroral plasma (unpublished manuscript), 1987.

Chevalier, M. W., W. B. Peter, U. S. Inan, T. F. Bell, and M. Spasojevic, Remote sensing of ionospheric disturbances associated with energetic particle precipitation using the south pole vlf beacon, *J. Geophys. Res.*, *112*(A11), 11,306, doi:10.1029/2007JA012425, 2007.

Gurnett, D. A., and R. R. Anderson, *The Kilometric Radio Emission Spectrum: Relationship to Auroral Acceleration Processes*, *Geophysical Monograph*, vol. Physics of Auroral Arc Formation, AGU, 1981.

Gurnett, D. A., R. L. Huff, and D. L. Kirchner, The wide-band plasma wave investigation, *Space Sci. Rev.*, *79*, 195–208, 1997.

James, H. G., E. L. Hagg, and L. P. Strange, Narrowband radio noise in the topside ionosphere, in *Non-Linear Effects in Electromagnetic Wave Propagation*, no. 138 in Conference Pre-Prints, North Atlantic Treaty Organization, Advisory Group for Aerospace Research & Development, 7 Rue Ancelle, 92200, Neuilly Sur Seine, France, 1974.

James, H. G., E. P. King, A. White, R. H. Hum, W. H. H. L. Lunscher, and C. L. Siefring, The e-pop radio receiver instrument on cassiope, *Space Sci. Rev.*, 2015.

Kletzing, C. A., W. S. Kurth, M. Acuna, R. J. MacDowall, R. B. Torbert, T. Averkamp, D. Bodet, S. R. Bounds, M. Chutter, J. Connerney, D. Crawford, J. S. Dolan, R. Dvorsky, G. B. Hospodarsky, J. Howard, V. Jordanova, R. A. Johnson, D. L. Kirchner, B. Mokrzycki, G. Needell, J. Odom, D. Mark, J. R. F. Pfaff, J. R. Phillips, C. W. Piker, S. L. Remington, D. Rowland, O. Santolik, R. Schnurr, D. Sheppard, C. W. Smith, R. M. Thorne, and J. Tyler, The electric and magnetic field instrument suite and integrated

science (emfisis) on rbsp, *Space Sci. Rev.*, *179*, 127–181, doi:10.1007/s11214-013-9993-6, 2013.

Kodera, K., R. Gendrin, and C. de Villedary, Complex representation of a polarized signal and its application to the analysis of ulf waves, *J. Geophys. Res.*, *82*(7), 1245–1255, 1977.

LaBelle, J., and R. R. Anderson, Ground-level detection of auroral kilometric radiation, *Geophys. Res. Lett.*, *38*(4), doi:10.1029/2010GL046411, 2011.

LaBelle, J., and R. A. Treumann, Poynting vector measurements of electromagnetic ion cyclotron waves in the plasmasphere, *J. Geophys. Res.*, *97 (A9)*(13), 789–797, 1992.

LaBelle, J., and R. A. Treumann, Auroral radio emissions, 1. hisses, roars, and bursts, *SSR*, *101*(3, 4), 295–440, 2002.

LaBelle, J., M. L. Trimpi, R. Brittain, and A. T. Weatherwax, Fine structure of auroral roar emissions, *J. Geophys. Res.*, *100*(A11), 21,953–21,959, 1995.

LaBelle, J., A. T. Weatherwax, M. Tantiwiwat, E. Jackson, and J. Linder, Statistical studies of auroral mf burst emissions observed at south pole station and at multiple sites in northern canada, *J. Geophys. Res.*, *110*(A2), doi:10.1029/2004JA010608, 2005.

LaBelle, J., X. Yan, M. C. Broughton, S. Pasternak, M. P. Dombrowski, R. R. Anderson, H. U. Frey, A. T. Weatherwax, and Y. Ebihara, Further evidence for a connection between auroral kilometric radiation and ground-level signals measured in antarctica, *J. Geophys. Res.*, *120*(3), 2061–2075, doi:10.1002/2014JA020977, 2015.

Makita, K., *VLF-LF Hiss Emissions Associated with Aurora*, *Memoirs of National Institute of Polar Research: Aeronomy*, vol. 16, National Institute of Polar Research, 1979.

Martin, L. H., Observations of 'whistlers' and 'chorus' at the south pole, *Nature*, *187*, 1018–1019, doi:10.1038/1871018a0, 1960.

Patterson, J. D., T. P. Armstrong, C. M. Laird, D. L. Detrick, and A. T. Weatherwax, Correlation of solar energetic protons and polar cap absorption, *J. Geophys. Res.*, *106*(A1), 149–163, doi:10.1029/2000JA002006, 2001.

Rodger, A. S., and T. J. Rosenberg, Riometer and hf radar signatures of polar patches, *Radio Science*, *34*(2), 501–508, doi:10.1029/1998RS900005, 1999.

Samara, M., J. LaBelle, C. A. Kletzing, and S. R. Bounds, Rocket observations of structured upper hybrid waves at fuh = 2fce, *Geophys. Res. Lett.*, *31*(22), 2004.

Sato, Y., T. Ono, N. Sato, and Y. Ogawa, First observations of $4f_{ce}$ auroral roar emissions, *Geophys. Res. Lett.*, *39*(7), 2012.

Sato, Y., A. Kadokura, Y. Ogawa, A. Kumamoto, and Y. Katoh, Polarization observations of $4f_{ce}$ auroral roar emissions, *Geophys. Res. Lett.*, *42*(2), 249–255, 2015.

Sazhin, S. S., K. Bullough, and M. Hayakawa, Auroral hiss: a review, *Planetary and Space Science*, *41*(2), 153–166, 1993.

Shepherd, S. G., J. LaBelle, and M. L. Trimpi, The polarization of auroral radio emissions, *Geophys. Res. Lett.*, *24*(24), 3161–3164, 1997.

Shepherd, S. G., J. LaBelle, R. A. Doe, M. McCready, and A. T. Weatherwax, Ionospheric structure and the generation of auroral roar, *J. Geophys. Res.*, *103*(A12), 29,253–29,266, 1998a.

Shepherd, S. G., J. LaBelle, and M. L. Trimpi, Further investigation of auroral roar fine structure, *J. Geophys. Res.*, *103*(A2), 2219–2229, 1998b.

Yan, X., J. LaBelle, G. Haerendel, M. Spasojevic, N. L. Bunch, D. I. Golden, H. U. Frey, and A. T. Weatherwax, Dayside auroral hiss observed at south pole station, *J. Geophys. Res.*, *118*(3), 1220–1230, doi:10.1002/jgra.50141, 2013.

Ye, S., J. LaBelle, and A. T. Weatherwax, Further study of flickering auroral roar emission: 1. south pole observations, *J. Geophys. Res.*, *111*(A7), doi:10.1029/2005JA011271, 2006.

Ye, S., J. LaBelle, P. H. Yoon, and A. T. Weatherwax, Experimental tests of the eigenmode theory of auroral roar fine structure and its application to remote sensing, *J. Geophys. Res.*, *112*(A12304), doi:10.1029/2007JA012525, 2007.

Yoon, P. H., A. T. Weatherwax, and J. LaBelle, Discrete electrostatic eigenmodes associated with ionospheric density structure: Generation of auroral roar fine frequency structure, *J. Geophys. Res.*, *105*(A12), 27,589–27,596, 2000.